Self-assembly of Rubrene on Copper Surfaces

Jill A. Miwa,[†] Fabio Cicoira,[†,‡,§] Stéphane Bedwani,[||] Josh Lipton-Duffin,[†] Dmitrii F. Perepichka,[⊥] Alain Rochefort,[||] and Federico Rosei*,[†]

Centre Énergie, Matériaux et Télécommunications, Institut National de la Recherche Scientifique, Université du Québec, 1650 Boulevard Lionel-Boulet, Varennes, J3X 1S2, Québec, Canada, Département de génie physique et Regroupement québécois sur les matériaux de pointe (RQMP), École Polytechnique de Montréal, Montréal, H3C 3A7, Québec, Canada, Department of Chemistry, McGill University, 801 Sherbrooke Street West, Montreal, H3A 2K6, Québec, Canada, Department of Material Science and Engineering, Bard Hall, Cornell University, Ithaca, New York 14853−1501, and Institute of Photonics and Nanotechnology, Consiglio Nazionale delle Ricerche Via alla Cascata 56/c 38050 Povo (Trento), Italy

Received: March 31, 2008; Revised Manuscript Received: April 15, 2008

We report a detailed investigation of the self-assembly of the organic semiconductor rubrene on low-index (100) and (110) facets of copper by scanning tunneling microscopy (STM) and supported by density functional theory (DFT) calculations. Rubrene adsorbs in orientations depending on substrate symmetry, resulting in different self-assembled motifs. STM images point to an asymmetric adsorption geometry, and DFT calculations further suggest that the molecule adsorbs in a twisted conformation.

Introduction

The adsorption properties and self-assembly of organic molecules on metal surfaces have been intensely investigated for over a decade.[1–21] Besides their value in terms of fundamental understanding, such studies are important for the development of future hybrid nanoelectronic devices based on single molecules or self-assembled molecular thin films where organic/inorganic interfaces play a major role.[22] Molecular self-assembly at surfaces is determined by surface chemistry, surface orientation, surface anisotropy, molecular conformational flexibility, and in some cases the nonplanarity of the molecules.[5,14,17,23]

Rubrene (5,6,11,12-tetraphenyltetracene, $C_{42}H_{28}$) was first synthesized over 80 years ago.[24] Its molecular structure was debated in the early literature,[25,26] but has now been established by X-ray crystallography.[27] It has excellent electronic properties and is being extensively employed in organic electronic devices such as light-emitting diodes[28–30] and field-effect transistors (FETs).[31–38] Rubrene is a benchmark material for single crystal organic FETs, as its hole field-effect mobility is among the highest observed in organic semiconductors ($\leq$15 cm^2/Vs).[33,35,38] This exceptionally high carrier mobility is attributed to efficient cofacial $\pi-\pi$ stacking in the single crystal.[33,39] A hole mobility as high as 2.5 cm^2/Vs has recently been achieved in rubrene thin film transistors.[40] The excellent charge transport properties of rubrene have motivated several fundamental studies of rubrene single crystals,[27–42] thin films,[43–47] and self-assembled structures.[28,48–50]

Rubrene is a nonplanar and flexible molecule consisting of a tetracene backbone with two pairs of phenyl substituents symmetrically attached on either side of the backbone (Figure 1). The intramolecular steric hindrance between the phenyl substituents results in a significant strain within the molecule,

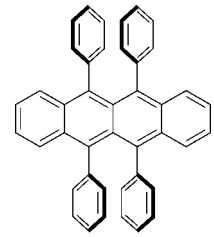

Figure 1. Chemical structure of rubrene.

which can be released by either a twisting of the tetracene backbone as seen in the gas phase geometry (Figure 2, conformation A), or by an out-of-plane distortion of the phenyl substituents seen in the single crystal geometry (Figure 2, conformation B). The twisting of the tetracene backbone renders the molecule chiral.

Recent near edge X-ray adsorption fine structure (NEXAFS) experiments performed on vacuum-deposited rubrene thin films on Au(111) and SiO_2[45] demonstrated that the tetracene backbone remains twisted upon deposition of the first few monolayers on these surfaces, whereas the backbone becomes planar (Figure 2, conformation B) at higher coverages. This change is induced by the increased contribution of the rubrene lattice, which supplies the energy for backbone planarization. The self-assembly of rubrene has recently been studied by scanning tunneling microscopy (STM) on Au(111) at 5 K.[48] These studies suggested that, upon adsorption, the molecule maintains its twisted conformation and therefore its chirality. Further studies demonstrated that rubrene on Au(111) exhibits adsorption geometries with differing electronic properties.[49] A previous STM study by our group has demonstrated the use of a Cu/Cu−O periodic supergrating as a nanotemplate to guide the assembly of rubrene.[51]

A detailed understanding of the adsorption and self-assembly of rubrene on metal surfaces, particularly those used for electrodes, is important for controlling the formation of rubrene thin films, which is required for exploring the potential of this molecule for ordered nanoscale structures as well as for

* Corresponding author e-mail: (F.R.) rosei@emt.inrs.ca, (A.R.) alain.rochefort@polymtl.ca, (F.C.) fc87@cornell.edu.
[†] Université du Québec.
[‡] Cornell University.
[§] Institute of Photonics and Nanotechnology.
[||] École Polytechnique de Montréal.
[⊥] McGill University.

10.1021/jp802762q CCC: $40.75
Published on Web 06/14/2008

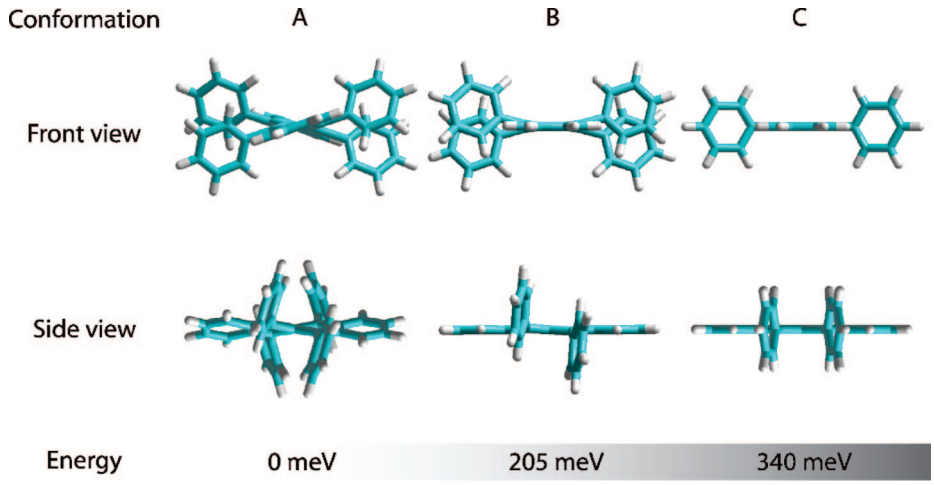

Figure 2. Calculated DFT/LDA energies for three different rubrene conformations. Conformation A represents rubrene in the gas phase, which is the lowest energy state. In its crystalline form, rubrene conforms to model B, requiring an energy of 205 meV to deform the molecule from the gas phase configuration. Straightening of the phenyl side groups costs an additional 135 meV and results in conformation C. The energy needed for a transition from the completely twisted conformation A to the straight conformation C is at least 340 meV.

optimizing its use in organic electronics devices. In this work, we investigate the adsorption and self-assembly of rubrene on the (100) and (110) facets of copper, a metal that is often used as electrode material. Using STM and density functional theory (DFT) calculations we find that, at room temperature, rubrene self-assembles on these surfaces into highly ordered motifs that reflect the symmetry of the substrate. Individual rubrene molecules within a given self-assembled pattern on either surface are imaged with contrast localized at the lateral phenyl substituents. Our experiments and calculations also demonstrate that rubrene adsorbs on Cu in a twisted conformation, due to its configurational flexibility.

Experimental Section

Rubrene adsorption on copper was studied in ultrahigh vacuum (UHV) with a variable temperature STM, furnished with standard equipment for sample preparation and characterization (Omicron GmbH, Germany). The base pressure of the system is $<5 \times 10^{-11}$ mbar. The Cu single crystals (Matek GmbH, Germany) were cleaned by repeated cycles of 600 eV Ar^+ sputtering and annealing to ~825 K. After several hours of degassing, rubrene (Aldrich, purity 99%) was evaporated from a Knudsen cell at temperatures ranging from 430−450 K onto surfaces held at ~300 K. STM images were acquired at room temperature with a chemically etched W tip. Typical imaging parameters were ≈ −2.0 V bias voltage and 0.5 nA tunneling current; the negative voltage indicates that the sample is biased negatively with respect to the tip (filled states). In general, switching to positive biases had little impact on the appearance of the molecules but often resulted in a less stable tunneling junction. Therefore, the majority of the presented images are filled state images. The images were acquired from the topographic channel and were subsequently analyzed using the free WSxM software.[52] Overlayer unit cells were determined from STM data, approximating lattice vector magnitudes to the nearest substrate lattice point. Measured distances and angles were determined to within ± 5%, the uncertainties arising chiefly from thermal drift and piezo creep. The DFT calculations were performed using the GAMESS software package.[53] Calculations for an isolated rubrene molecule and for a single rubrene adsorbed on Cu(100) were performed using the Local Density Approximation (LDA), employing Huzinaga minimal basis sets for carbon and hydrogen atoms and a LANL2DZ effective core potential (ECP) for copper atoms. The Cu(100) surface was modeled as a single layer cluster containing 30 atoms in which the interatomic distance was fixed to the bulk value of 2.56 Å. The geometry of the copper cluster was fixed during the calculations whereas the geometry of rubrene was fully optimized using a quasi-Newton method until a gradient convergence factor better than 10^{-5} Hartree/Bohr was reached. The optimized DFT/LDA geometries of rubrene on Cu(100) were used to produce the STM simulations, using the recently developed SPAGS-STM (Strongly Parallel Adaptive Grid Solvers−STM) software that is based on a STM simulation technique originally developed by Cerdá et al.[54]

Results and Discussion

Geometry Optimization of Isolated Rubrene. The energy of the various conformations of isolated gas phase rubrene molecules was computed using DFT, and optimized geometries are presented in Figure 2. Conformation A is highly twisted and is the optimum geometry in the gas phase. Conformation B, which closely resembles the conformation in the single crystal, has a planar tetracene backbone and tilted side groups. Our calculations indicate that this conformation is 205 meV less stable than A, in agreement with a previously reported X-ray absorption spectroscopy and thermal desorption spectroscopy study.[45] Conformation C has a planar backbone and straight side groups and is 135 meV less stable than B. However, this conformation has never been experimentally observed. We note that the energy penalties involved in these conformational changes are considerably lower than the typical adsorption energy of a few electronvolts; hence, conformational changes are expected to occur upon adsorption.

Rubrene Adsorption and Self-assembly. On Cu(100), rubrene self-assembles into a highly ordered herringbone-like pattern (Figure 3b). Individual rubrene molecules within the self-assembled network appear as two bright elongated lobes separated by a dark region. On the basis of the calculated dimensions of a single molecule on Cu(100), we attribute each lobe to a pair of phenyl substituents and the enclosed dim region to the tetracene backbone. This appearance suggests that rubrene is adsorbed with its backbone parallel to the Cu surface, an adsorption geometry that maximizes the interaction between the metal surface and the π orbitals of the molecule. Our calculations yield a width (W) of 0.87 nm, as measured from the center of

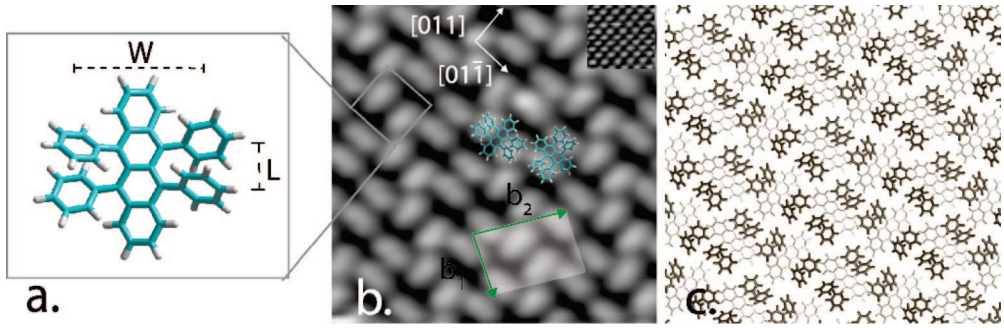

Figure 3. Self-assembled domain of rubrene on Cu(100). (a) Width (W) and length (L) parameters defined for a single rubrene molecule. (b) High resolution (8.0 × 8.0 nm^2) STM image of the herringbone structure (I_t = 0.36 nA, V_s = 2.05 V). One overlayer unit cell is shown. The inset (2.0 × 2.0 nm^2) shows the underlying (100) surface with atomic resolution (I_t = 0.93 nA, V_s = −0.32 V). The surface unit cell is indicated by the gray box. (c) A model of the entire STM image shown in panel b. Because the contrast is localized at the phenyl substituents, we assume that the backbone makes minimal contributions to the local density of states, so the substituents in the model are highlighted in black.

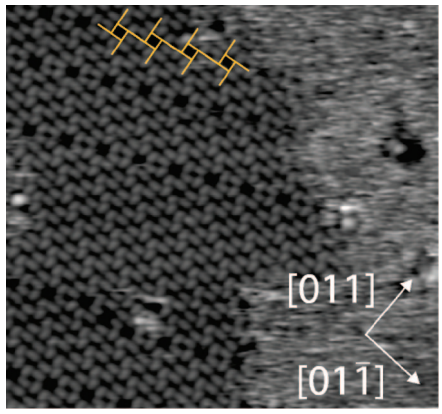

Figure 4. STM image of rubrene domains that are tens of nanometers wide (31.6 × 31.6 nm^2). Pinwheel structures formed at domain boundaries are highlighted by the orange markers (I_t = 0.36 nA, V_s = 2.05 V).

one phenyl ring across the short axis of the tetracene backbone to the center of the opposing phenyl ring (Figure 3a). The length (L), defined as the distance between centers of paired phenyl substituents on the same side of the backbone, was calculated by DFT to be 0.34 nm. Respective width and length measurements of 0.84 ± 0.04 nm and 0.34 ± 0.02 nm were obtained from STM images and are in agreement with the calculations (Figure 9).

Within the herringbone structure, molecules are aligned along the principal [011] and [01$\bar{1}$] directions of the surface. These equivalent adsorption geometries reflect the c_4 symmetry of the surface. A model is proposed in Figure 3c. The resulting molecular packing density of the herringbone structure is 0.55 molecules/nm^2, as determined from STM images. The unit cell of the adsorbate structure is shown in Figure 3b. The overlayer lattice vectors, $\vec{b}_1$ and $\vec{b}_2$, have magnitudes 1.47 ± 0.07 nm and 2.4 ± 0.1 nm, respectively, and the angle between the vectors is 89 ± 4°. In matrix notation, this structure is described as follows.

$$\begin{pmatrix} 4 & -3 \\ 4 & 7 \end{pmatrix}$$

In this model (as well as in those for rubrene on Cu(110) shown later in Figure 7) we propose adsorption sites where the fused rings of the tetracene backbone are centered on the top sites that could maximize the interaction between the molecule and the metal.[55] This is a tentative model because the exact registry of rubrene with the surface could not be determined by STM. The precise local registry with the surface was not successfully determined since atomic resolution could not be obtained in the presence of rubrene islands.

An interesting feature of the self-assembly of rubrene on Cu(100) is the formation of "pinwheels" consisting of four rubrene molecules, which appear at domain boundaries. One of these boundaries is highlighted with orange markers at the top of Figure 4. The pinwheel structures are formed by a shift in position of neighboring domains, as illustrated by the models in Figure 5. Figure 5a shows rubrene molecules arranged in a herringbone pattern where domain I (shaded gray) and II coincide. A shift in position of domain II by $2\vec{a}_2 - 1\vec{a}_1$, where $\vec{a}_1$ and $\vec{a}_2$ are the Cu substrate lattice vectors, produces a pinwheel (highlighted by the orange makers in Figure 5b). The direction and magnitude of the black arrow represents the straight translation of the molecules colored red, blue, and green of domain II, with respect to domain I. The hollow black dot indicates the position of the red colored rubrene molecule of the untranslated domain II in Figure 5a. The four molecules that define a single pinwheel are the two molecules (black) of domain I and the red and blue molecules of domain II. Domains typically extend for tens of nanometers. However, in some cases the domains are so small that they consist only of boundaries. Regions of the surface of a few square nanometers can be entirely occupied by the pinwheel motif. These structures illustrate the important fact that the domains are chiral. Two enantiomorphic regions separated by a mirror plane are illustrated in Figure 6. In the left image, the pinwheels appear in a clockwise orientation (orange markers), and in the image to the right the pinwheels are arranged in a counterclockwise orientation. The inherent asymmetry of the unit cell itself explains this phenomenon, as a mirror-reflected unit cell described by the following matrix,

$$\begin{pmatrix} 3 & -4 \\ 7 & 4 \end{pmatrix}$$

which places molecules at identical lattice sites, adequately describes the second enantiomorph. Furthermore, we note that each of the domains is composed of a single rubrene enantiomorph.

When deposited on Cu(110), rubrene molecules may self-assemble into one of two highly ordered patterns, both of which occur simultaneously on the surface in domains that are typically tens of nanometers wide. The patterns are consistent with the c_2 symmetry of the surface, and we refer to them as the "box" structure (Figure 7, panels a and c) and the "zigzag" structure (Figure 7, panels b and d). Individual rubrene molecules within

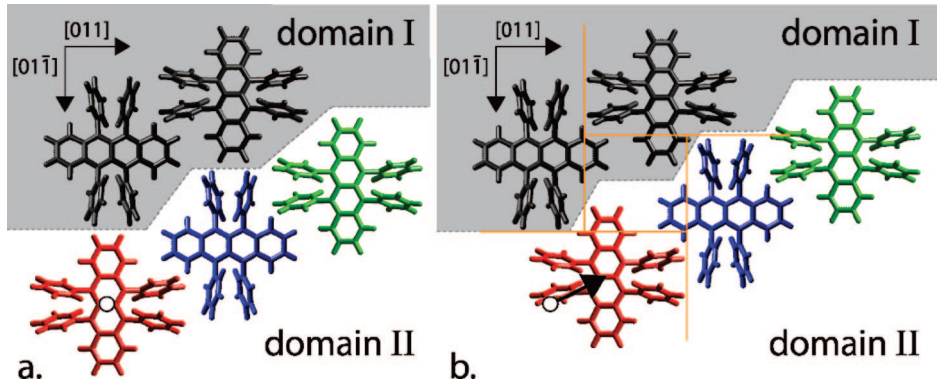

Figure 5. Pinwheel formation. (a) When domains I and II coincide, the molecules form a herringbone pattern. The boundary between the two domains is highlighted by the dashed gray line. (b) The molecules (red, blue, and green) of domain II are shifted by the distance and direction indicated by the black arrow, whereas the molecules (black) of domain I (shaded gray) remain in the same position as in panel a. The hollow black dot indicates the position of the red rubrene molecule of the untranslated domain II in panel a. The straight translation of domain II, with respect to domain I, results in the formation of a pinwheel that is highlighted by the orange markers. The two black rubrene molecules of domain I and the red and blue rubrene molecules of domain II comprise a single pinwheel.

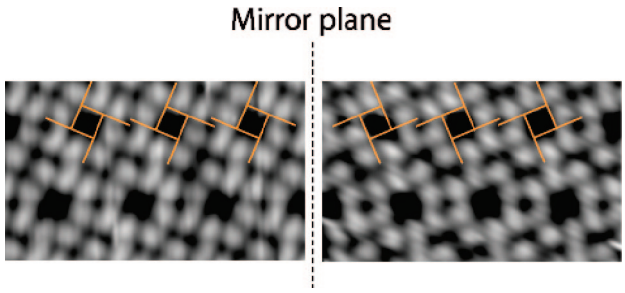

Figure 6. STM images of two enantiomorphic domains of rubrene on Cu(100). The dashed line corresponds to a mirror plane. Clockwise pinwheels are found in the left panel and counterclockwise ones are shown at the right. Left image: $V_s = 2.22$ V, $I_t = 0.34$ nA, 9.9×5.8 nm^2; right image: $V_s = 1.93$ V, $I_t = 0.25$ nA, 9.8×5.8 nm^2.

both structures are imaged as four bright lobes surrounding a dimmer region. Width and length dimensions of 0.86 ± 0.04 and 0.39 ± 0.05 nm, respectively, were obtained from STM images and are in agreement with their respective values of 0.85 and 0.35 nm as determined from DFT calculations for an isolated rubrene molecule on Cu(110).

The box structure consists of rows of molecules running along the [001] crystal lattice direction. All of the molecules within a given [001] row are aligned in the same direction. However, the molecules within the row are oriented perpendicular to those within adjacent rows. Therefore, the backbones of the molecules are aligned either along the [001] or [$\bar{1}$10] directions. The inter- and intrarow periodicities are 2.2 ± 0.1 and 1.46 ± 0.07 nm, respectively. The molecular centers of rubrenes in adjacent rows are staggered with respect to one another by half the intrarow periodicity (i.e., 0.72 ± 0.04 nm, which is consistent with two lattice spacings of the Cu substrate). Thus, the rectangular unit cell for this molecular arrangement can be described in matrix notation as follows,

$$\begin{pmatrix} 8 & 0 \\ 0 & 4 \end{pmatrix}$$

or as $c(8 \times 4)$ in Wood's notation. The unit cell and lattice vectors ($\vec{c}_1$ and $\vec{c}_2$) are superimposed on the STM image shown in Figure 7c, and a tentative model of the structure is depicted in Figure 7e. STM images that simultaneously resolve both rubrene islands and the underlying [$\bar{1}$10] rows of the Cu surface (Figure 8) indicate that the backbones aligned with the [$\bar{1}$10] direction reside on top of the atomic rows, as previously observed for unsubstituted oligoacenes and oligothiophenes on Cu(110).[55–59]

The zigzag structure also consists of rows running along the [001] direction. However, every molecule in this structure is oriented with its backbone aligned along [$\bar{1}$10]. The separation between neighboring molecules along the [001] and [$\bar{1}$10] directions is 2.2 ± 0.1 and 1.55 ± 0.08 nm, respectively. As with the box structure, the molecular centers of rubrene molecules in neighboring rows are shifted by half of the intrarow periodicity (i.e., 1.12 ± 0.06 nm, or three Cu lattice spacings) with respect to one another. The primitive cell for the zigzag structure is rhombic, as described by the following matrix,

$$\begin{pmatrix} 3 & 3 \\ 3 & -3 \end{pmatrix}$$

but can also be described by the nonprimitive cell $c(6 \times 6)$ in Wood's notation. A model of this structure is displayed in Figure 7f.

The molecular packing densities are 0.60 molecules/nm^2 for the box structure and 0.45 molecules/nm^2 for the zigzag structure. The close packing of the molecules within the box structure should make the overall network quite stable, and the commensurability of the tetracene backbone with the [$\bar{1}$10] direction of the surface should lend stability to the zigzag structure. These competing effects may explain why both types of structures always appear to coexist on the surface.

The noisy regions surrounding the islands likely arise from adsorbate diffusion on the surface (Figure 7, panels a and b). We do not observe isolated molecules outside of the molecular ensembles, which is further evidence that any molecules not contained in the structured islands are highly diffusive.[60,61] Islands are observed after a threshold coverage of approximately 0.7 monolayers (ML) is reached. Similar behavior has been observed for other π-conjugated hydrocarbons on other metallic surfaces, for example, perylene on Ag(110)[62] and Cu(100),[56] coronene on Cu(100),[63] and complex helical molecules such as heptahelicene on Cu(111).[64] STM imaging of dynamic changes at the boundaries of the rubrene islands confirms an exchange of molecules taking place between diffusing rubrene molecules on the surface and the self-assembled structures.

An issue of particular interest is to determine if the molecules' distorted conformation in the gas phase and the consequent chirality are retained upon adsorption, as is the case of rubrene

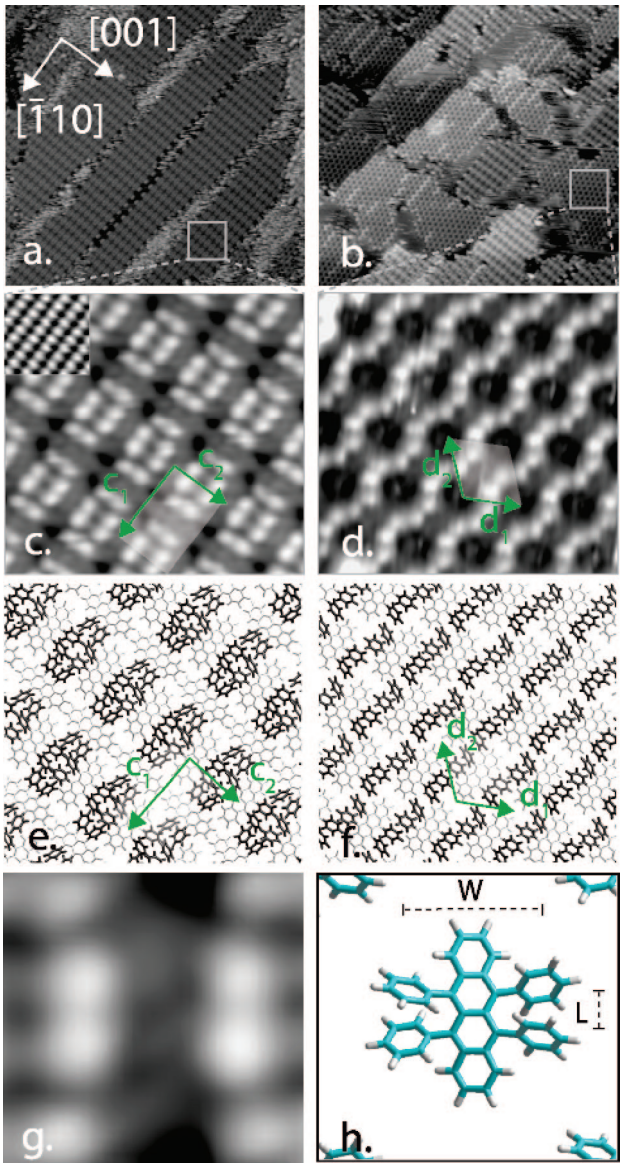

Figure 7. Self-assembled domains of rubrene on Cu(110). Large scale (70×70 nm^2) STM images of (a) the box structure ($V_s = -1.97$ V, $I_t = 0.34$ nA) and (b) the zigzag structure ($V_s = -1.58$ V, $I_t = 0.42$ nA). High resolution image (7×7 nm^2) of (c) the box structure ($V_s = -0.53$ V, $I_t = 0.34$ nA) and (d) the zigzag structure ($V_s = -1.9$ V, $I_t = 0.30$ nA). The lattice vectors and unit cells for both structures are shown. The inset in (c) shows the underlying copper lattice 2×2 nm^2, $I_t = 1.28$ nA and $V_s = -0.37$ V. A model of the box structure, corresponding to the STM image in panel c, is depicted in panel e. Similarly, a model of the zigzag structure corresponding to the STM image in panel d is shown in panel f. In panel g, a STM image of a molecule within the box structure. In panel h, a rubrene model corresponding to the image in panel g.

on Au(111).[48] The STM images obtained on Cu(100) suggest that the tetracene backbone of the molecule lies parallel to the surface. To gain further insight into the molecules' conformation we analyzed series of apparent height profiles of the phenyl substituents of rubrene molecules adsorbed on Cu(100). Figure 9 shows a distinct asymmetry in the heights of the substituents; height profiles taken across the short axis of the tetracene backbone (i.e., the width of the molecule) indicate that the top left phenyl ring is higher than the top right one (brown profile), and the bottom left one is lower than the bottom right phenyl ring (green profile). Similarly, length profiles demonstrate that the top left phenyl ring is higher than the bottom left phenyl

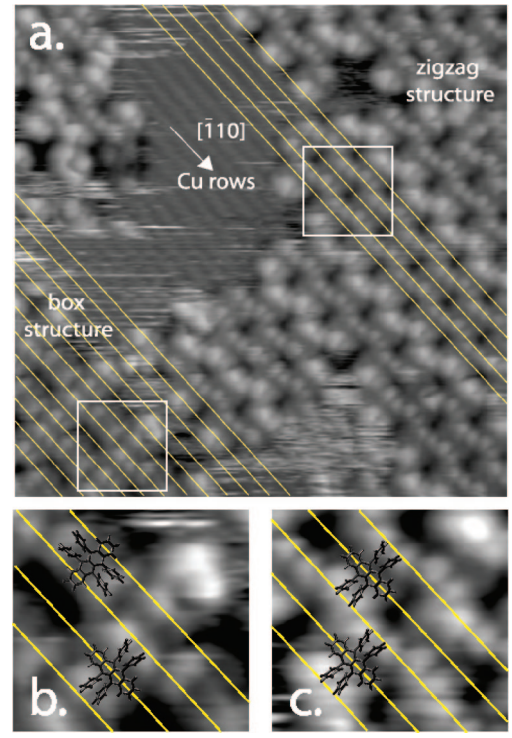

Figure 8. STM image of the underlying [$\bar{1}$10] copper rows and both rubrene polymorphs ($V_s = 1.89$ V, $I_t = 0.51$ nA, 20×20 nm^2). The yellow lines are aligned with copper rows and are superimposed on the self-assembled structures to determine the position of the tetracene backbone with respect to the copper rows. Molecular models are superimposed on both structures. The gray boxes highlight the box (b) and zigzag (c) structures (4×4 nm^2).

ring (red profile) and the top right is lower than the bottom right phenyl ring (blue profile). The difference in height is of the order of tenths of Ångstroms but is consistent across hundreds of molecules in images acquired at different voltages ranging from 0.5 to 2.5 V. Further confirmation is provided by STM simulations that predict similar height differences. This demonstrates that the asymmetry is indeed a topographic effect and not an electronic one. Therefore, we can conclude that, despite their planar appearance in the STM images, rubrene molecules adsorb in a nonplanar conformation. STM simulations support the preference of a twisted adsorption geometry. This is clearly evident in the height profiles produced from the simulation shown in the lower left corner of Figure 9.

The STM simulation was generated modeling an individual rubrene molecule with a twisted conformation on Cu(100); its calculated torsion angles are reported in Figure 10. The tetracene backbone of adsorbed rubrene is slightly less twisted (36°) than that of rubrene in the gas phase (40°). However, the torsion angle between the side-end phenyl substituents is significantly smaller (13°) in the adsorbed state than in the gas phase (36°) and single crystal (25°). Consequently, the difference in height between two phenyl substituents located on the same side of the backbone of an adsorbed rubrene is expected to decrease upon adsorption, in agreement with the small height differences measured in Figure 9. On the basis of height profiles and torsion angle calculations, we conclude that the rubrene backbone remains twisted upon adsorption, and the molecule therefore retains its chirality.

DFT calculations for a rubrene molecule on Cu(110) yield a geometry that is very similar to the one found on the Cu(100) surface. The calculated adsorption energies for a single rubrene molecule on Cu(110) and Cu(100) are 3.3 eV and 4.3 eV,

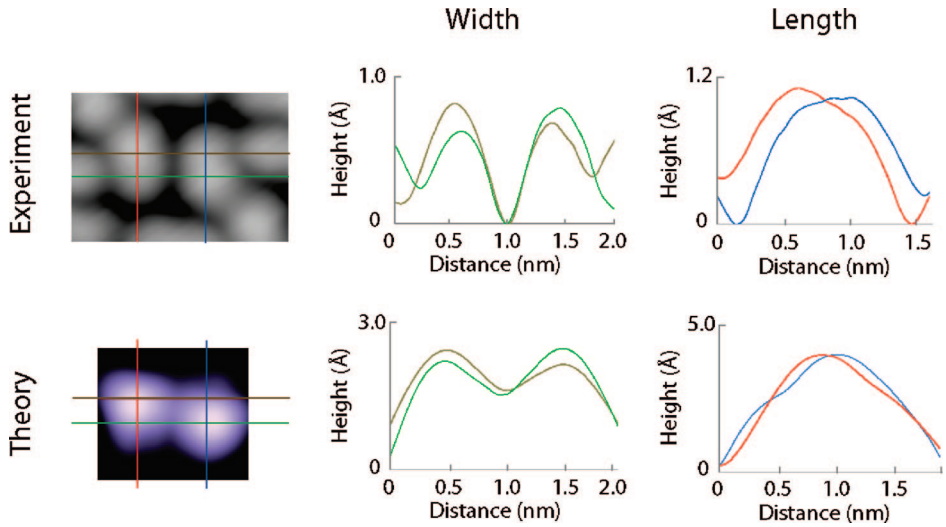

Figure 9. Measured height profiles of the phenyl substituents for a single rubrene molecule adsorbed on Cu(100) (top) and corresponding generated profiles from STM simulations (bottom). Experimental image: $V_s = 2.05$ V, $I_t = 0.36$ nA, 2.61×2.12 nm^2, and simulated image: $V_s = 2.0$ V, $I_t = 0.36$ nA, 2.01×1.80 nm^2.

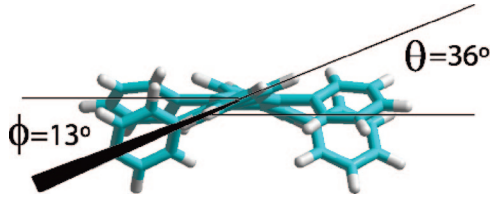

Figure 10. Front view highlighting the torsion angle of the tetracene backbone (θ) and the torsion angle between the phenyl rings of the side-end substituents (ϕ) for a single rubrene molecule adsorbed the Cu(100) surface.

respectively. Although adsorption energies are usually overestimated using the LDA,[65] the calculated values are qualitatively similar to experimentally determined adsorption energies of 2.1 eV for pentacene on Cu(110)[66] and 0.73 eV for benzene on Cu(110).[67] STM height profiles of rubrene molecules within both types of structures on Cu(110) indicate an asymmetric adsorption geometry (Figure 11), and DFT calculations suggest that the molecules adsorb in a twisted conformation. Simulated STM images for rubrene on Cu(110) are similar to those for Cu(100), where a single molecule appears as two large bright lobes. However, for both rubrene polymorphs on Cu(110), the STM resolves the lateral phenyl substituents individually, and the tetracene backbone is visible, although with much weaker contrast. The differences might arise from the fact that the simulations are performed for individual molecules at 0 K, whereas STM images were acquired for molecules tightly packed into self-assembled networks, at room temperature.

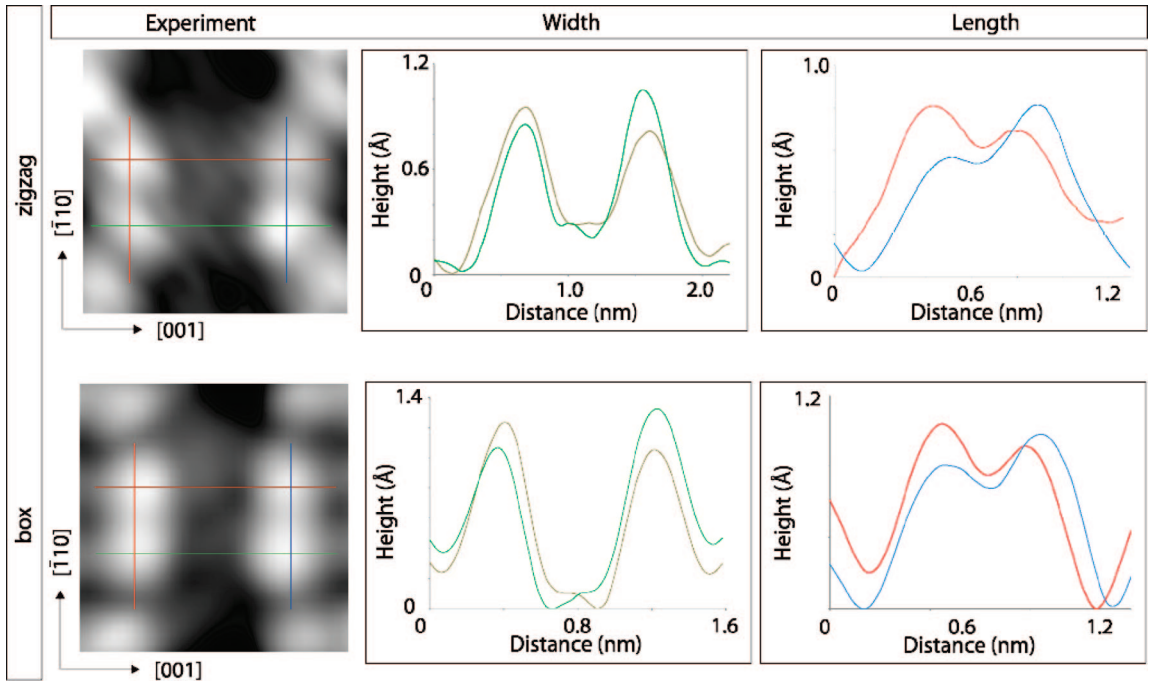

Figure 11. STM images of an individual rubrene within the zigzag (top) and box (bottom) structures. Measured height profiles taken across the width (brown and green) and length (red and blue) of the molecule are shown to the right of the images. A pronounced asymmetry of the phenyl groups can be seen for both types of profiles. Image parameters for zigzag and box images are $V_s = -1.90$ V, $I_t = 0.30$ nA, 1.6×1.6 nm^2 and $V_s = -0.53$ V, $I_t = 0.34$ nA, 1.6×1.6 nm^2, respectively.

Therefore the difference in appearance could be due to thermally induced rotations of the phenyl groups about the C−C bond and intramolecular interactions within the self-assembled network.

Conclusions and Perspectives

Rubrene self-assembles on the (100) and (110) facets of copper into highly ordered structures where individual molecules are aligned along the high symmetry directions of the substrate. Individual rubrene molecules in a given self-assembled pattern are imaged with high contrast localized at the lateral phenyl substituents, and thus the tetracene backbone minimally contributes to the local density of states near the Fermi level.

We observe self-assembled patterns that depend on substrate symmetry. On Cu(100), which has c_4 symmetry, we find a single self-assembled pattern with a chiral unit cell that is emphasized by the formation of chiral pinwheel motifs at domain boundaries. On the reduced-symmetry (c_2) Cu(110) facet we observe two distinct self-assembled patterns (i.e., box and zigzag) where the molecules are oriented along the [$\bar{1}$10] or [001] surface directions.

Height measurements performed by STM and supporting DFT calculations indicate that rubrene adsorbs with a twisted geometry. However, the torsion angle between the side-end phenyl substituents is smaller in the adsorbed state than in the gas phase.

Our results are of paramount importance for understanding the self-assembly and thin film growth of rubrene, a material that is expected to play a key role in future organic electronic devices. To gain deeper understanding, angle-resolved photoemission spectroscopy studies would provide useful information about the electronic hybridization of the rubrene orbitals in contact with the metallic surface,[68] provided that large single domains were grown. Moreover, further scanning probe studies of substituted rubrenes could provide insight into how substituents with different stereochemistry can modify the self-assembly properties.

Acknowledgment. This work was partly supported by INRS start up funds and by NSERC of Canada. F.C. acknowledges the European Union under the project MC OIF 040864-TOPOS. F.R. is grateful to FQRNT and the Canada Research Chairs program for partial salary support. D.F.P. and F.R. acknowledge financial support from an FQRNT "équipe" grant, from the Petroleum Research Fund (American Chemical Society) and from the Air Force Office of Scientific Research of the USA We also acknowledge the Centre for Self Assembled Chemical Structures (CSACS). We thank C. Santato for helpful discussions.

References and Notes

(1) Rosei, F. *J. Phys.: Condens. Matter* **2004**, *16*, S1373.
(2) Witte, G.; Wöll, Ch. *J. Mater. Res.* **2004**, *19*, 1889.
(3) Barth, J. V. *Annu. Rev. Phys. Chem.* **2007**, *58*, 375.
(4) Barth, J. V.; Costantini, G.; Kern, K. *Nature* **2005**, *437*, 671.
(5) Rosei, F.; Schunack, M.; Naitoh, Y.; Jiang, P.; Gourdon, A.; Lægsgaard, E.; Stensgaard, I.; Joachim, C.; Besenbacher, F. *Prog. Surf. Sci.* **2003**, *71*, 95.
(6) Ernst, K. H. *Top. Curr. Chem.* **2006**, *265*, 209.
(7) De Feyter, S.; De Schryver, F. *Top. Curr. Chem.* **2005**, *258*, 205.
(8) Tomba, G.; Lingenfelder, M.; Costantini, G.; Kern, K.; Klappenberger, F.; Barth, J. V.; Ciacchi, L. C.; De Vita, A. *J. Phys. Chem. A* **2007**, *111*, 12740.
(9) Theobald, J.; Oxtoby, N.; Phillips, M.; Champness, N.; Beton, P. *Nature* **2003**, *424*, 1029.
(10) Henzl, J.; Bredow, T.; Morgenstern, K. *Chem. Phys. Lett.* **2007**, *435*, 278.
(11) Hipps, K.; Scudiero, L.; Barlow, D.; Cooke, M. *J. Am. Chem. Soc.* **2001**, *124*, 2126.
(12) Smith, C. B.; Makha, M.; Raston, C. L.; Sobolev, A. N. *New J. Chem.* **2007**, *31*, 535.
(13) Hallmark, V. M.; Chiang, S.; Brown, J. K.; Wöll, C. *Phys. Rev. Lett.* **1991**, *66*, 48.
(14) Frommer, J. *Angew. Chem., Int. Ed.* **1992**, *31*, 1298.
(15) Jung, T. A.; Schlittler, R. R.; Gimzewski, J. K.; Tang, H.; Joachim, C. *Science* **1996**, *271*, 181.
(16) Rabe, J. P. *Adv. Mater.* **1989**, *8*, 299.
(17) Chiang, S. *Chem. Rev.* **1997**, *97*, 1083.
(18) Lippel, P. H.; Wilson, R. J.; Miller, M. D.; Wöll, Ch.; Chiang, S. *Phys. Rev. Lett.* **1989**, *62*, 171.
(19) Cicoira, F.; Santato, C.; Rosei, F. *Top. Curr. Chem.* **2008**, in press.
(20) Pivetta, M.; Blüm, M. C.; Patthey, F.; Schneider, W. D. *Angew. Chem., Int. Ed.* **2008**, *120*, 1092.
(21) Zheng, Y.; Dongchen, Q.; Chandrasekhar, N.; Xingyu, G.; Troadec, C.; Wee, A. T. S. *Langmuir* **2007**, *23*, 8336.
(22) Nitzan, A.; Ratner, M. A. *Science* **2003**, *300*, 1384.
(23) Shi, D.; Ji, W.; Lin, X.; He, X.; Lian, J.; Gao, L.; Cai, J.; Lin, H.; Du, S.; Lin, F.; Seidel, C.; Chi, L.; Hofer, W.; Fuchs, H.; Gao, H. J. *Phys. Rev. Lett.* **2006**, *96*, 226101.
(24) Moureu, C.; Dufraisse, C.; Dean, P. *C. R. Hebdomad. Séances Acad. Sci.* **1926**, *182*, 1440.
(25) Bergmann, F.; Herlinger, E. *J. Chem. Phys.* **1936**, *4*, 532.
(26) Schonberg, A. *J. Am. Chem. Soc.* **1936**, *58*, 182.
(27) Jurchescu, O. D.; Meetsma, A.; Palstra, T. T. M. *Acta Crystallogr., Sect. B: Struct. Sci.* **2006**, *62*, 330.
(28) Sakamoto, G.; Adachi, C.; Koyama, T.; Taniguchi, Y.; Merritt, C. D.; Murata, H.; Kafafi, Z. H. *Appl. Phys. Lett.* **1999**, *75*, 766.
(29) Aziz, H.; Popovic, Z. D. *Appl. Phys. Lett.* **2002**, *80*, 2180.
(30) Li, G.; Shinar, J. *Appl. Phys. Lett.* **2003**, *83*, 5359.
(31) Podzorov, V.; Sysoev, S. E.; Loginova, E.; Pudalov, V. M.; Gershenson, M. E. *Appl. Phys. Lett.* **2003**, *83*, 3504.
(32) Stassen, A. F.; de Boer, R. W. I.; Iosad, N. N.; Morpurgo, A. F. *Appl. Phys. Lett.* **2004**, *85*, 3899.
(33) Sundar, V. C.; Zaumseil, J.; Podzorov, V.; Menard, E.; Willett, R. L.; Someya, T.; Gershenson, M. E.; Rogers, J. A. *Science* **2004**, *303*, 1644.
(34) Podzorov, V.; Menard, E.; Borissov, A.; Kiryukhin, V.; Rogers, J. A.; Gershenson, M. E. *Phys. Rev. Lett.* **2004**, *93*, 086602.
(35) Takeya, J.; Yamagishi, M.; Tominari, Y.; Hirahara, R.; Nakazawa, Y.; Nishikawa, T.; Kawase, T.; Shimoda, T.; Ogawa, S. *Appl. Phys. Lett.* **2007**, *90*, 102120.
(36) Briseno, A. L.; Mannsfeld, S. C. B.; Ling, M. M.; Liu, S. H.; Tseng, R. J.; Reese, C.; Roberts, M. E.; Yang, Y.; Wudl, F.; Bao, Z. N. *Nature* **2006**, *444*, 913.
(37) Takahashi, T.; Takenobu, T.; Takeya, J.; Iwasa, Y. *Appl. Phys. Lett.* **2006**, *88*, 033505.
(38) Zeis, R.; Besnard, C.; Siegrist, T.; Schlockermann, C.; Chi, X. L.; Kloc, C. *Chem. Mater.* **2006**, *18*, 244.
(39) da Silva, D. A.; Kim, E. G.; Bredas, J. L. *Adv. Mater.* **2005**, *17*, 1072.
(40) Hsu, C.; Deng, J.; Staddon, C.; Beton, P. *Appl. Phys. Lett.* **2007**, *91*, 193505.
(41) Menard, E.; Marchenko, A.; Podzorov, V.; Gershenson, M. E.; Fichou, D.; Rogers, J. A. *Adv. Mater.* **2006**, *18*, 1552.
(42) Luo, Y.; Gustavo, F.; Henry, J. Y.; Mathevet, F.; Lefloch, F.; Sanquer, M.; Rannou, P.; Grevin, B. *Adv. Mater.* **2007**, *19*, 2267.
(43) Kowarik, S.; Gerlach, A.; Sellner, S.; Schreiber, F.; Pflaum, J.; Cavalcanti, L.; Konovalov, O. *PhysChemChemPhys* **2006**, *8*, 1834.
(44) Wang, L.; Chen, S.; Liu, L.; Qi, D. C.; Gao, X. Y.; Wee, A. T. S. *Appl. Phys. Lett.* **2007**, *90*, 132121.
(45) Käfer, D.; Ruppel, L.; Witte, G.; Wöll, Ch. *Phys. Rev. Lett.* **2005**, *95*, 166602.
(46) Käfer, D.; Witte, G. *PhysChemChemPhys* **2005**, *7*, 2850.
(47) Ribi, P. R.; Bratina, G. *J. Phys. Chem. C* **2007**, *111*, 18558.
(48) Blüm, M. C.; Cavar, E.; Pivetta, M.; Patthey, F.; Schneider, W. D. *Angew. Chem., Int. Ed.* **2005**, *44*, 5334.
(49) Blüm, M. C.; Pivetta, M.; Patthey, F.; Schneider, W. D. *Phys. Rev. B* **2006**, *73*, 195409.
(50) Ribi, P. R.; Bratina, G. *Surf. Sci.* **2007**, *601*, L25.
(51) Cicoira, F.; Miwa, J. A.; Perepichka, D. F.; Rosei, F. *J. Phys. Chem. A* **2007**, *111*, 12674.
(52) Horcas, I.; Fernandez, R.; Gomez-Rodriguez, J. M.; Colchero, J.; Gomez-Herrero, J.; Baro, A. M. *Rev. Sci. Instrum.* **2007**, *78*, 013705.
(53) Schmidt, M. W.; Baldridge, K. K.; Boatz, J. A.; Elbert, S. T.; Gordon, M. S.; Jensen, J. H.; Koseki, S.; Matsunaga, N.; Nguyen, K. A.; Su, S.; Windus, T. L.; Dupuis, M.; Montgomery, J. A. *J. Comput. Chem.* **1993**, *14*, 1347.
(54) Cerdá, J.; Van Hove, M. A.; Sautet, P.; Salmeron, M. *Phy. Rev. B* **1997**, *56*, 15885.
(55) Chen, Q.; McDowall, A. J.; Richardson, N. V. *Langmuir* **2003**, *19*, 10164.

(56) Chen, Q.; Rada, T.; McDowall, A.; Richardson, N. V. *Chem. Mater.* **2002**, *14*, 743.

(57) Chen, Q.; McDowall, A. J.; Richardson, N. V. *Chem. Mater.* **2003**, *15*, 4113.

(58) Kang, J. H.; Zhu, X. Y. *Chem. Mater.* **2006**, *18*, 1318.

(59) Cicoira, F.; Miwa, J. A.; Melucci, M.; Barbarella, G.; Rosei, F. *Small* **2006**, *2*, 1366.

(60) Busse, C.; Weigelt, S.; Petersen, L.; Lægsgaard, E.; Besenbacher, F.; Linderoth, T. R.; Thomsen, A. H.; Nielsen, M.; Gothelf, K. V. *J. Phys. Chem. B* **2007**, *111*, 5850.

(61) Schunack, M.; Petersen, L.; Kuhnle, A.; Lægsgaard, E.; Stensgaard, I.; Johannsen, I.; Besenbacher, F. *Phys. Rev. Lett.* **2001**, *86*, 456.

(62) Deng, Z. T.; Lin, H.; Ji, W.; Gao, L.; Lin, X.; Cheng, Z. H.; He, X. B.; Lu, J. L.; Shi, D. X.; Hofer, W. A.; Gao, H. J. *Phys. Rev. Lett.* **2006**, *96*, 156102.

(63) Richardson, N. V. *New J. Phys.* **2007**, *9*, 395.

(64) Fasel, R.; Parschau, M.; Ernst, K. H. *Angew. Chem., Int. Ed.* **2003**, *42*, 5178.

(65) Salahub, D. R. *Adv. Chem. Phys.* **1987**, *69*, 447.

(66) Baldacchini, C.; Mariani, C.; Betti, M. G. *J. Chem. Phys.* **2006**, *124*, 154702.

(67) Lomas, J. R.; Baddeley, C. J.; Tikhov, M. S.; Lambert, R. M. *Langmuir* **1995**, *11*, 3048.

(68) Ferretti, A.; Baldacchini, C.; Calzolari, A.; Di Felice, R.; Ruini, A.; Molinari, E.; Betti, M. G. *Phys. Rev. Lett.* **2007**, *99*, 046802.

JP802762Q